Numerical simulation of natural convection between two infinite differentially heated vertical plates

Zhenlan Gao[1,2], Bérengère Podvin[2], Anne Sergent[1,2], Shihe Xin[3], Patrick Le Quéré[2], & Laurette S. Tuckerman[4]

[1] UPMC Univ Paris 06, 75005 Paris
[2] LIMSI-CNRS, 91403 Orsay
[3] CETHIL, INSA de LYON, 69621 Villeurbanne
[4] PMMH (ESPCI-CNRS-UPMC-UPD), 75005 Paris

gao@limsi.fr

Résumé. Nous étudions les instabilités de convection naturelle d'une lame d'air ($Pr = 0.71$) comprise entre deux plaques verticales infinies différentiellement chauffées. La température de chaque plaque est constante et uniforme. Nous nous appuyons sur des simulations numériques directes 3D au voisinage du nombre de Rayleigh critique. L'écoulement autour de la première bifurcation est comparé aux prédictions d'une équation de Ginzburg-Landau dérivée analytiquement. Les bifurcations successives et brisures de symétries associées sont analysées et identifiées.

Abstract. We consider the natural convection of air ($Pr = 0.71$) between two infinite vertical differentially heated plates. The temperature on each plate is constant and uniform. We use a 3D direct numerical simulation (DNS) code to determine the instabilities of the flow above the critical Rayleigh number. A Ginzburg-Landau equation is derived analytically for the flow around the first bifurcation and its predictions are compared to DNS results. Subsequent bifurcations and associated symmetry-breaking phenomena are analyzed and identified.

1 Introduction

Instability of natural convection in a vertical fluid layer between two vertical differentially heated plates is of substantial interest for many industrial applications, such as heat exchangers in reactors or insulation of buildings (e.g. double-paned windows). The first experiments were carried out by Elder [1]. Gill and Davey[2] and Bergholz [3] investigated the linear stability of two-dimensional convection between vertical plates. Mizushima and Gotoh [4] used a weakly nonlinear approach to represent the flow. Mizushima and Saito [5] used 2D direct numerical simulation to compute the nonlinear equilibrium states of secondary convection with a Newton-Raphson method. Nagata and Busse [6], Clever and Busse [7] computed the secondary, tertiary and quaternary solutions in the limit of vanishing Prandtl number. In the present paper we consider the three-dimensional flow between two infinite, vertical, differentially heated plates. We use a 3D direct numerical simulation (DNS) code [8] to examine how the flow becomes progressively less organized as the Rayleigh number increases. We derive a Ginzburg-Landau equation to represent the flow around the first bifurcation. We then describe the subsequent bifurcations of the flow and associated symmetry breaking phenomena.

2 Physical problem, equations of motion and numerical configuration

2.1 Physical problem

We consider the air flow between two infinite vertical plates maintained at different temperatures. The configuration is represented in Fig. 1. The distance between the two plates is D, the periodic height and depth of the plates are H and L_y respectively. The temperature difference between the plates is set to be ΔT. The x direction is normal to the plates, and the gravity g is in the $-z$ direction.

(a) Study domain   (b) Base flow profiles
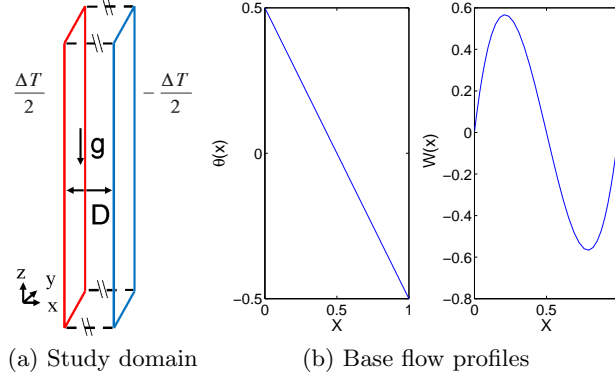
Figure 1. Study domain and base flow profiles for the temperature θ and vertical velocity W.

The relevant fluid properties are the viscosity ν, thermal conductivity κ, and coefficient of the thermal expansion β. Four nondimensional parameters characterize the flow : the Prandtl number $Pr = \nu/\kappa$, two aspect ratios $A_y = L_y/D$ and $A_z = H/D$, and the Rayleigh number based on the gap between the two plates $Ra = \frac{g\beta\Delta T D^3}{\nu\kappa}$. Only the Rayleigh number dependence is considered in the present study. The Prandtl number is fixed and equal to 0.71. The two periodic lengths are set to be $A_y = 1$ and $A_z = 10$.

2.2   Equations of motion

The flow is governed by the Navier-Stokes equations within the Boussinesq approximation. The equations are nondimensionalized with the reference parameters $\frac{\kappa}{D}\sqrt{Ra}$ for the velocity, D for the length, and ΔT for the temperature. t denotes time, $\underline{u} = (U, V, W)$ is the velocity vector, p is the pressure and θ is the reduced temperature.

$$\nabla \cdot \underline{u} = 0 \tag{1}$$

$$\frac{\partial \underline{u}}{\partial t} + \underline{u} \cdot \nabla \underline{u} = -\frac{1}{\rho_0}\nabla p + \frac{Pr}{\sqrt{Ra}}\Delta \underline{u} + Pr\theta\hat{z} \tag{2}$$

$$\frac{\partial \theta}{\partial t} + \underline{u} \cdot \nabla \theta = \frac{1}{\sqrt{Ra}}\Delta \theta \tag{3}$$

with Dirichlet boundary conditions at the plates

$$\underline{u}(0, y, z, t) = \underline{u}(1, y, z, t) = 0, \quad \theta(0, y, z, t) = 0.5, \quad \theta(1, y, z, t) = -0.5, \tag{4}$$

and periodic conditions in the y and z directions.

The equations of motion (1)-(4) admit an analytic steady solution, which depends only on the x direction :

$$W(x) = \frac{1}{6}\sqrt{Ra}\left((x - \frac{1}{2})^3 - \frac{1}{4}(x - \frac{1}{2})\right), \qquad \theta(x) = -(x - \frac{1}{2}) \tag{5}$$

The base flow is represented in Fig. 1b. The temperature profile corresponds to the pure conduction case. The equations (1)-(4) admit an $O(2) \times O(2)$ symmetry. One $O(2)$ symmetry corresponds to the translations in the transverse direction y and the reflection $y \to -y$, while the other corresponds to the translations in the vertical direction z and a reflection that combines centrosymmetry and Boussinesq symmetry : $(x, z, T) \to (-x, -z, -T)$.

2.3   Numerical configuration

The simulations are carried out with a multi-domain spectral code [8]. A Chebyshev discretization is applied in directions x and z, while a Fourier discretization is used in the direction y. The equations are integrated in time with a second-order mixed explicit-implicit scheme. The initial condition is typically taken to be the base flow. We use 30 modes in the transverse direction y, and 40 and 160 modes in the horizontal and vertical, x and z, directions, respectively.

3   Results

3.1   First bifurcation

DNS results The first bifurcation in the DNS occurs at $Ra_c \sim 5800$, and is characterized by the appearance of four 2D steady corotating rolls which are represented in figure 2(a),(b). Although vertical invariance is broken, the solution stills displays the symmetry D_4, consisting of translation by the height $A_z/4$ of each of the rolls, and the centro-Boussinesq symmetry. Invariance of the equations under z-translations ensures that there exists a whole circle of solutions, corresponding to an arbitrary vertical translation of the rolls : the bifurcation is a circle pitchfork bifurcation.

The time evolution of the temperature measured at the point $(0.0381, 0.097, 5)$, which is in the boundary layer next to the hot wall, is plotted in Fig. 3a. An enlargement of the same signal for the times $1500 < t < 2000$ is represented in logarithmic scale in Fig. 3b. The temperature disturbance grows exponentially for $1500 < t < 1750$, which corresponds to the linear growth of the most unstable eigenmode, then increases at a slower rate for $t > 1750$ before the amplitude of the solution saturates. As was pointed out in [9], this evolution shows that the coefficient of the cubic term in the normal form of the circle pitchfork bifurcation is negative, and therefore that the bifurcation is supercritical.

(a)   (b) 2D st   (c) 3D st   (d) 3D $t = 2001$ (e) 3D $t = 2010$ (f) 3D $t = 2020$ (g) 3D $t = 2029$
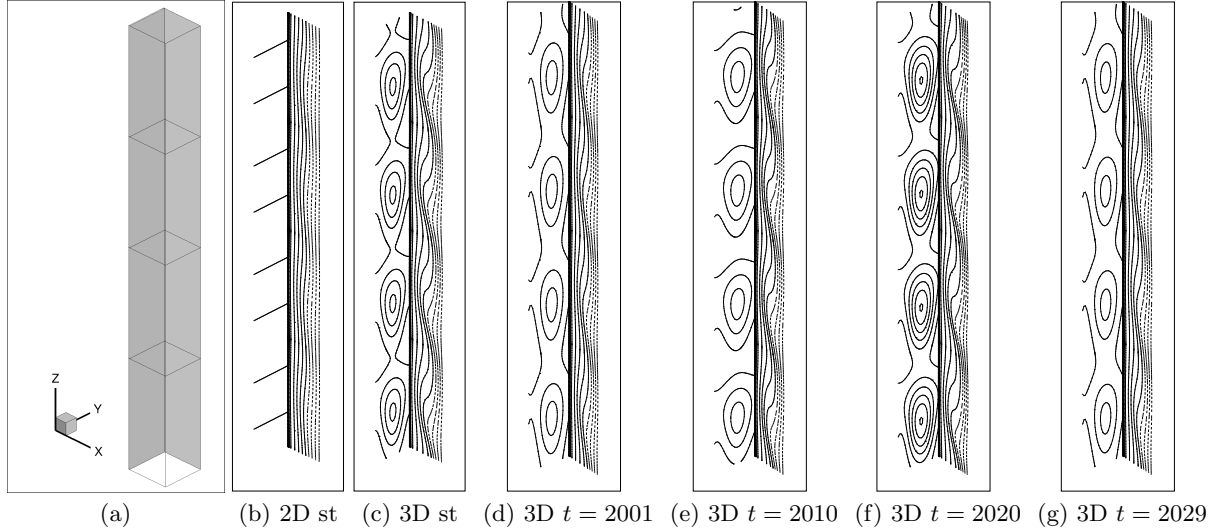
Figure 2. Flow structures : iso-contours of temperature on two selected vertical planes. (a) Positions of the selected planes $x = 0.0245$ (close to the hotter wall) and $y = 0.9677$ (perpendicular to side-walls) (b) 2D steady (st) four-roll pattern at $Ra = 6000$; (c) 3D steady pattern at $Ra = 11000$; (d)-(g) 3D time-dependent pattern at $Ra = 11500$ at different instants.

(a)   (b)   (c)   (d)
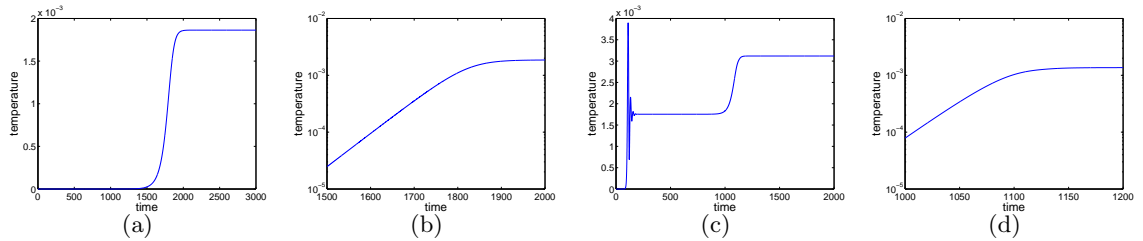
Figure 3. Time series of temperature at the point $(0.038, 0.097, 5)$: (a) $Ra = 6000$; (b) enlargement of (a) for $1500 < t < 2000$ on a logarithmic scale; (c) $Ra = 11000$; (d) enlargement of (c) for $1000 < t < 1200$.

Linear stability analysis The base flow (5) is parallel and depends only on the x-direction. The hypotheses of Squire's theorem are verified, so that the most unstable mode is expected to be 2D. Let ψ be the stream function and θ the temperature.

The 2D system of perturbations in x and z is written as

$$M\frac{\partial \phi}{\partial t} = L\phi + b(\phi, \phi) \tag{6}$$

with

$$\phi = \begin{bmatrix} \psi \\ \theta \end{bmatrix}; \ b = \begin{bmatrix} b_\phi \\ b_\theta \end{bmatrix}; \ M = \begin{bmatrix} \nabla^2 & 0 \\ 0 & 1 \end{bmatrix}; \quad L = \begin{bmatrix} \frac{Pr}{\sqrt{Ra}}\nabla^4 - W\frac{\partial}{\partial z}\nabla^2 + \frac{\partial^2 W}{\partial x^2}\frac{\partial}{\partial z} & Pr\frac{\partial}{\partial x} \\ \frac{\partial \Theta}{\partial x}\frac{\partial}{\partial z} & \frac{1}{\sqrt{Ra}}\nabla^2 - W\frac{\partial}{\partial z} \end{bmatrix} \tag{7}$$

where the nonlinear terms are defined as

$$b_\psi(\phi_\alpha, \phi_\beta) = \left(\frac{\partial \psi_\alpha}{\partial z}\frac{\partial}{\partial x} - \frac{\partial \psi_\alpha}{\partial x}\frac{\partial}{\partial z}\right)\nabla^2 \psi_\beta \qquad b_\theta(\phi_\alpha, \phi_\beta) = \left(\frac{\partial \psi_\alpha}{\partial z}\frac{\partial}{\partial x} - \frac{\partial \psi_\alpha}{\partial x}\frac{\partial}{\partial z}\right)\theta_\beta. \tag{8}$$

The linear part of the system is equivalent to a generalized eigenvalue problem $L\phi = \sigma M\phi$. Solution of the eigenvalue problem leads to values for the critical Rayleigh number $Ra_c = 5708$ and the critical wavenumber $k_c = 2.81$, which agree with [3] and [10]. The modulus of the most unstable mode at the critical wavenumber k_c and Rayleigh number Ra_c is shown in Fig. 4a. One can see that the intensity of the modes is maximum in the mid-plane between the two plates.

Weakly nonlinear analysis We use a multiscale analysis to derive a Ginzburg-Landau equation for the flow around the first bifurcation. The flow solution is written as $(\psi, \theta) = A(\tilde{\psi}, \tilde{\theta})e^{ikz}$, where $\tilde{\psi}, \tilde{\theta}$ are the most unstable modes at the wavenumber k_c given by the linear stability analysis, and A is the amplitude of the solution. We define the time scales : $t_0 = t, t_1 = \epsilon t, t_2 = \epsilon^2 t$ and the length scales in z : $z_0 = z, z_1 = \epsilon z$, expand all the operators in system (6) with respect to the new variables, and collect the terms at different orders of ϵ. The problem at order ϵ simply coincides with the linear stability analysis. Collecting terms at order ϵ^2 and imposing a compatiblity condition yields an expression for the group velocity C_g. Numerical evalution of C_g yields a value of about 10^{-5}, which is close to the expected value of zero since the rolls are steady. Another compatibility condition at order ϵ^3 leads to a Ginzburg-Landau equation [11] for the amplitude A,

$$\frac{\partial A}{\partial t} = \sigma(Ra - Ra_c)A + \gamma\frac{\partial^2 A}{\partial z^2} - lA^2 A^* \tag{9}$$

Numerical evalution of the coefficients σ, γ, l for the critical wavenumber $k_c = 2.81$ gives $\sigma = 7.67 \cdot 10^{-5}$, $\gamma = 0.112$, $l = 18.7$. The sign of l confirms that the bifurcation is supercritical, as was inferred from the DNS. The steady amplitude A was then computed from the Ginzburg-Landau equation and compared to that observed in the DNS. Figs 4b and 4c show that the agreement between the model and the DNS was found to be very good over a wide range of Rayleigh numbers. We note that the wavenumber $k_{DNS} = 2.79$ found in the DNS differs slightly from the critical wavenumber $k_c = 2.81$ determined by linear stability analysis.

3.2   Higher bifurcations

When $Ra > Ra_{c2} \sim 10100$, the four-roll steady solution becomes unstable in the transverse direction, and a steady 3D pattern, shown in figure 2(c), appears through a second bifurcation, as was also found by [6] and [7]. The flow is no longer y-invariant, but owing to the invariance of the equations by transverse translations, this new bifurcation is also a circle pitchfork bifurcation. By the same argument as was
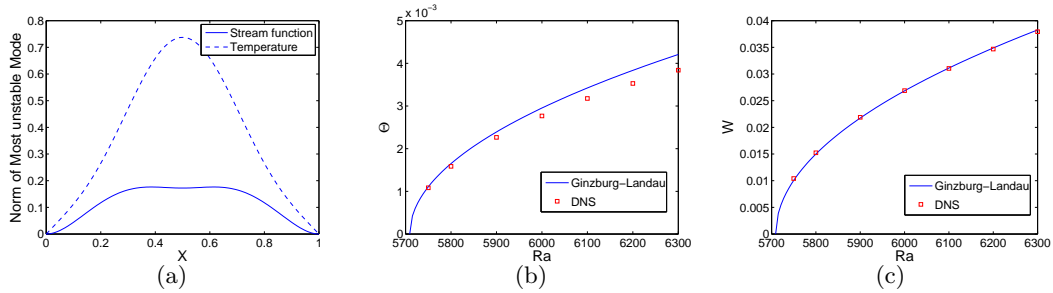
Figure 4. (a) Norm of the most unstable mode at k_c and Ra_c (b)-(c) comparison between the DNS and Ginzburg-Landau equation. b) maximum temperature c) maximum vertical velocity on the plane $x = 0.0381$.

used in the previous paragraph, the time series of Fig. 3d indicates that this is another supercritical bifurcation. The steady 3D solutions retain some of the symmetries of the 2D solutions, namely reflection in y and translation by $A_z/4$ in z, but the translation symmetry in y and the centro-Boussinesq symmetry are replaced by the single discrete symmetry $(x, y, z, T) \rightarrow (-x, y + 0.5, -z, -T)$. Thus, the $O(2) \times D_4$ symmetry of the 2D solution is replaced by $D_1 \times D_4$ for the 3D solution. The value of Ra_{c2} is obtained by integrating the linearized equations of motion and computing the growth rate of the y-dependent perturbation. We find that Ra_{c2} is about 9980.

The 3D pattern appears to be stable up to a value of $Ra = Ra_{c3} \sim 11300$. For $Ra_{c3} < Ra < 12000$, the 3D pattern becomes time-dependent as can be seen in Figs 2d- 2g. Only one frequency is detected at first, as shown in Figs 5a and 5b. The oscillation frequency is nearly independent of Ra over the interval $Ra_{c3} < Ra < 12000$, while the square of the oscillation amplitude increases linearly with Ra, which is consistent with a Hopf bifurcation. Extrapolation then leads to an estimate of 11270 for Ra_{c3}.
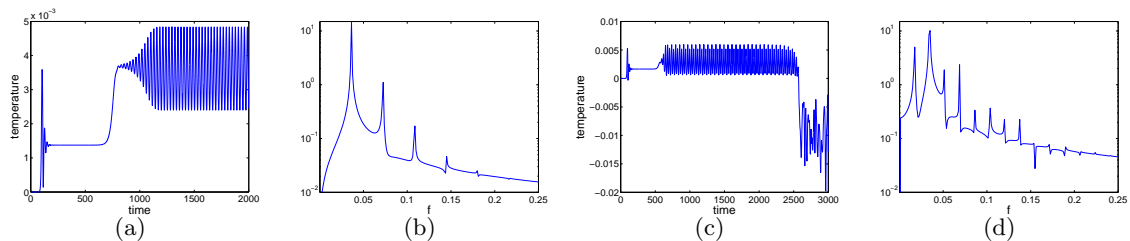
Figure 5. (a) Time series of temperature measured at the point (0.038, 0.097, 5) at $Ra = 11500$; (b) Temporal Fourier spectrum of the periodic portion portion ($t > 1000$) of the signal in a); (c) Temperature time series at $Ra = 12200$; (d) Temporal Fourier spectrum of the bi-periodic portion ($1000 < t < 2000$) of the signal in b).

When $12100 < Ra < 12500$, the oscillation period of the 3D pattern is doubled, as shown in Figs 5c, 5d at $Ra = 12200$ ($700 < t < 2500$). At larger times $t > 2500$, the oscillation becomes markedly irregular. This corresponds to a drastic change in the spatial organization of the flow, as the four oscillatory structures give way to an unsteady pattern of roughly three structures. For increasingly large values of Ra, successive period-doubling bifurcations are observed, as is apparent in the phase portraits shown in Fig. 6 for different Rayleigh numbers. Beyond $Ra = 13500$, it is no longer possible to identify a discrete set of frequencies and the flow appears temporally chaotic.

4   Conclusion

The goal of our study has been to determine the sequence of instabilities leading to chaos for the flow between two infinite, differentially heated vertical plates as the Rayleigh number increases. A partial

(a) $Ra = 12000$ (b) $Ra = 12100$ (c) $Ra = 12300$

(d) $Ra = 12310$ (e) $Ra = 12315$ (f) $Ra = 12320$
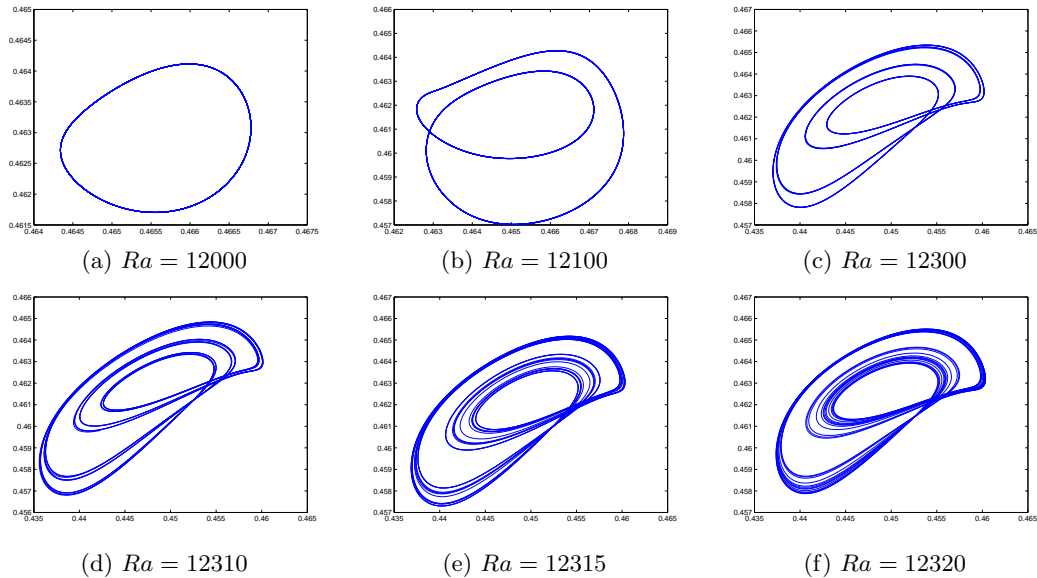
Figure 6. Phase portraits at different Ra. Abscissa : temperature measured at the point $(0.038, 0.097, 6.98)$; ordinate : temperature measured at the point $(0.038, 0.097, 6.54)$.

mapping of that route has now been established. The base flow first bifurcates to 2D steady rolls through a supercritical pitchfork bifurcation. A Ginzburg-Landau equation was derived analytically and was able to predict the amplitude of the 2D solution correctly. As the Rayleigh number increases, the 2D rolls become unstable through another supercritical pitchfork bifurcation to a steady 3D pattern, which itself becomes unstable to oscillatory 3D structures through a Hopf bifurcation. Chaos eventually occurs through a sequence of period-doubling bifurcations. A detailed investigation of the chaotic regime will be carried out in future work.

Références

1. J. W. ELDER, Laminar free convention in a vertical slot *Journal of Fluid Mechanics*, **23**, 77-98 (1965)
2. A. GILL, & A. DAVEY, Instability of a bouyancy-driven system *Journal of Fluid Mechanics*, **35**, 775-798 (1969)
3. R. F. BERGHOLZ, Instability of steady natural convection in a vertical fluid layer *Journal of Fluid Mechanics*, **84**, 743-768 (1978)
4. J. MIZUSHIMA, & K. GOTOH, Nonlinear evolution of the distubance in a vertical fluid layer *Journal of the Physical Society of Japan*, **52**, 1206-1214 (1983)
5. J. MIZUSHIMA & Y. SAITO, Equilibrium characteristics of the secondary convection in a vertical fluid layer between two flat plates, *Fluid Dynamics Research*, **2**, 193-191 (1987)
6. M. NAGATA, & F. H. BUSSE, Three-dimensional tertiary motions in a plane shear layer, *Journal of Fluid Mechanics*, **135**, 1-26 (1983)
7. R. M. CLEVER & F. H. BUSSE, Tertiary and quarternary solution for convection in a vertical fluid layer heated form the side, *Chaos, Solitons & Fractals*, **5**, 1795-1803 (1995)
8. S. XIN, J. CHERGUI, & P. LE QUÉRÉ, 3D Spectral Parallel Multi-Domain computing for natural convection flows *Proceedings at Parallel CFD 2008*, Université de Lyon, France. 163-170 (2008)
9. R. D. HENDERSON & D. BARKLEY, Secondary instability in the wake of a circular cylinder *Physics of Fluids*, **8**, 1683-1685 (1996)
10. A. GILL, & C. C. KIRKHAM, A note on the stability of convection in a vertical slot *Journal of Fluid Mechanics*, **42**, 125-127 (1970)
11. C. COSSU, *Introduction to hydrodynamic instabilities* Lecture Notes, École Polytechnique (2009)